UCRL- 97519
PREPRINT

Estimation of the Bulk Diffusivity of Chimneys using Post-Shot Holes

Norman R. Burkhard and Joseph R. Hearst
Lawrence Livermore National Laboratory

Jonathan M. Hanson
Hanson & Associates

This paper was prepared for submittal to
The Fourth Symposium on Containment
of Underground Nuclear Explosions
Held September 21-24, 1987

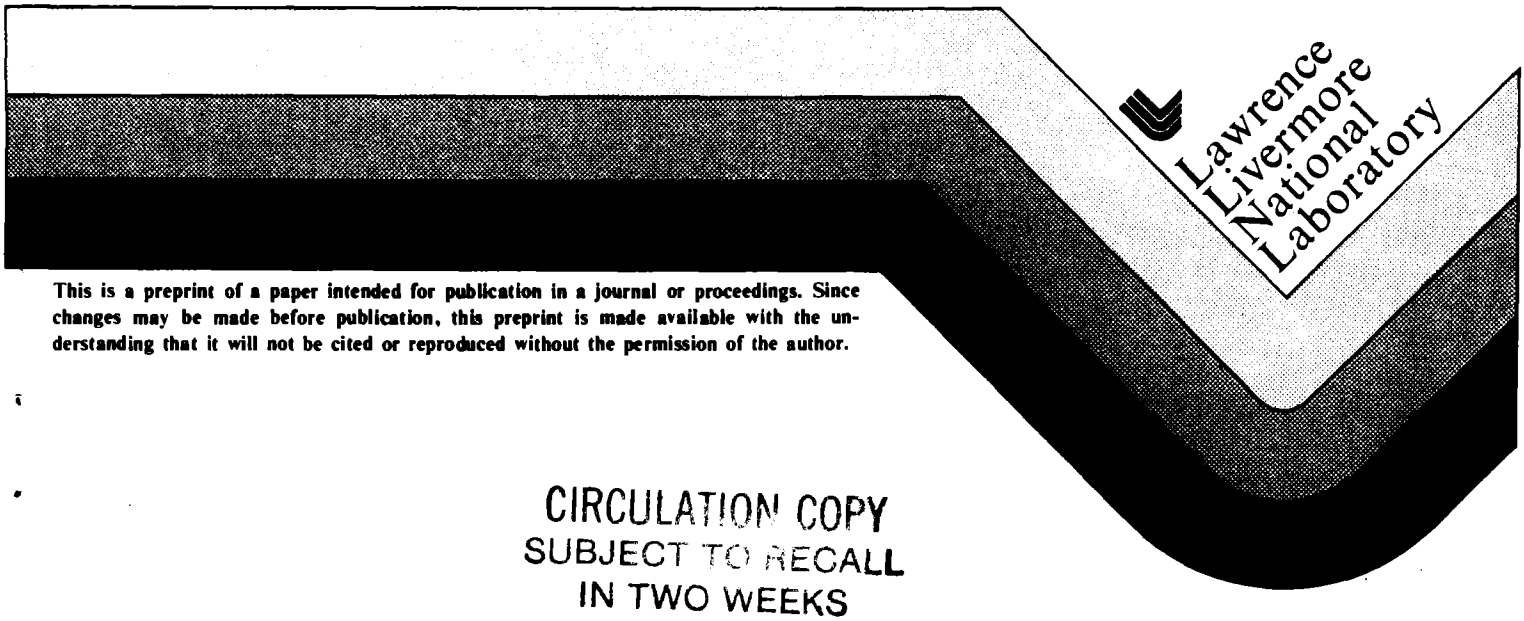

Estimation of the Bulk Diffusivity of Chimneys using Post-Shot Holes

Norman R. Burkhard and Joseph R Hearst
Lawrence Livermore National Laboratory
L-208, PO Box 808
Livermore, CA 94550

Jonathan M. Hanson
Hanson & Associates
PO Box 8047
Salt Lake City, UT 84108

Abstract

LLNL has been calculating the bulk diffusivity of chimney regions using measurements of atmospheric pressure variations. Fluctuations in atmospheric surface pressure and subsurface pressure (measured in a post-shot hole of opportunity) are compared to determine the diffusivity. The diffusivities calculated to date range from about 130 to 31000 m^2/hr. Time and frequency domain techniques have been utilized to determine this range of diffusivity Some limitations of this method of diffusivity determination have been discovered. Useful data have been obtained in the frequency band 0.002-0.03 cycles/hour. The effect of the water table upon our measurements has been determined. The theoretical impulse response functions for a typical geologic setting can be quite long (> 300 hours). Therefore, the surface pressure history for time spans greater than this or the entire initial pressure distribution (p(z,t=0)) in the geologic setting must be known before gas transport predictions from transport models can be reliably made, as the driving pressures for transport depend upon these initial conditions.

Introduction

The hydraulic diffusivity of the chimney and surrounding media can play an important role in the containment of radioactive gas generated during an underground nuclear explosion. Molecular diffusion of gas through the matrix or fractures, atmospheric pumping of gas to the surface, and steam-drive fracture extension depend upon the diffusivity and/or permeability. The stimulus for this work is a series of observations of late-time gas seepage from several sites on Pahute Mesa on the Nevada Test Site (NTS). We are now developing a data base of bulk diffusivity measurements in order to determine whether these sites are anomalous. Bulk diffusivity is our term for the diffusivity determined in a medium that contains both matrix and fractures. The importance of this parameter in the transport of radioactive gas to the surface is discussed by other investigators at this symposium [1,2]. In addition, we are attempting to determine whether it would be possible to predict the occurrence of late-time gas seepage from pre-shot measurements of diffusivity. The first step in our study is the determination of post-shot bulk diffusivity at many emplacement sites. This paper reports on this portion of the

study.

Lawrence Livermore National Laboratory (LLNL) has been making estimates pre-shot and post-shot of the diffusivity around emplacement holes. Estimates of the pre-shot diffusivity for alluvium and tuff sites were reported by Hanson and Hearst [3]. Since then, LLNL has developed a technique to estimate the diffusivity of the chimney and surrounding region using post-shot gas sampling holes. LLNL also did work on this problem in the early 1970's [4,5,6]. Interest in this work was rekindled by the observations of late-time seepage from several events.

The estimates of the diffusivity are obtained from atmospheric pressure measurements made simultaneously on the surface and downhole in the cavity region. Several time domain techniques and a frequency domain technique have been developed to obtain the estimates of diffusivity. As part of this process, analytical models for several simple cases have been derived. These models lead to a better understanding of the value and limitations of these measurements.

Theory

The hydraulic diffusivity of the medium combines the permeability and the porosity of the medium into one term in the diffusion equation:

$$\frac{\partial^2 p}{\partial z^2} = \frac{1}{C}\frac{\partial p}{\partial t} \qquad (1)$$

where $C = kp_0/\mu\varphi$ (2)

and where k = permeability
p_0 = static pressure
μ = viscosity of air
C = diffusivity
φ = porosity

and at normal atmospheric conditions, $C \approx 16\ k/\varphi$
with k in darcys,
and C in m^2/hr.

Solutions of this equation were formulated in the time domain using finite difference techniques. We have used the finite difference techniques to estimate the diffusivity of chimney regions at several different sites around NTS. In addition, we have obtained analytical solutions for the Green's function for this problem in the frequency domain for one dimensional horizontally homogeneous layered media as a tool in helping us understand the measurements and their possible limitations.

The Green's function is simply the impulse response of the system and is independent of either the surface or subsurface pressures. Examination of the characteristics of the Green's functions can help clarify fundamental properties of the diffusive system and reveal limitations that might occur in the interpretation of our pressure data sets to obtain diffusivity.

We have calculated the Green's function for the models illustrated in Figure 1. The

horizontally layered models use the appropriate combinations of the following boundary conditions for p(z,t) in their solution:

$$p(0,t) = \delta(t) \qquad \text{Surface condition for impulse response} \qquad (3)$$

$$\lim_{z \to \infty} p(z,t) = 0 \qquad \text{No pressure at infinity} \qquad (4)$$

$$\frac{\partial p(L,t)}{\partial z} = 0 \qquad \text{No flow at water table (z=L)} \qquad (5)$$

$$p_i(z=z_i,t) = p_{i+1}(z=z_i,t) \qquad \text{Continuity of pressure at layer boundary} \qquad (6)$$

$$k_i \frac{\partial p_i(z,t)}{\partial z} = k_{i+1} \frac{\partial p_{i+1}(z,t)}{\partial z} \qquad \text{No mass accumulation at layer boundary} \qquad (7)$$

The appropriate combinations of boundary conditions are used with Eq. 1 to obtain the Green's function for a homogeneous half space (with and without a water table) and a homogeneous layer over a half space (with and without a water table). These cases are illustrated in Figure 1. Assuming a time dependence of $\exp(-i\omega t)$, the solution to Eq. 1 for $p(z,\omega)$ in any layer can be represented as:

$$p_i(z,\omega) = A_i \exp(-\alpha_i z) + B_i \exp(\alpha_i z) \qquad (8)$$

$$\text{where } \alpha_i = \sqrt{-i\omega/C_i}$$

and where A_i and B_i depend on ω and are determined from the particular boundary conditions that apply to that problem and where C_i is the diffusivity.

The Green's function for a homogenous half space with no water table (solution to Equation 1 with boundary conditions 3 and 4) is:

$$G(z,\omega) = \exp(-\alpha z) \qquad (9)$$

The Green's function for a homogenous half space with a water table at z=L (solution to Equation 1 with boundary conditions 3 and 5) is:

$$G(z<L,\omega) = \frac{\cosh[\alpha(L-z)]}{\cosh(\alpha L)} \qquad (10)$$

The Greens' function solution for a homogeneous layer (thickness = H) over a homogeneous half space with no water table (solution to Equation 1 with boundary conditions 3, 4, 6, and 7) is:

$$G(z>H,\omega) = \frac{\exp(-\alpha_2 z)}{\exp(-\alpha_2 H)[\cosh(\alpha_1 H) + \kappa \sinh(\alpha_1 H)]} \qquad (11)$$

$$\text{where } \kappa = (k_2/k_1) \times \sqrt{C_1/C_2}$$

The analytical Green's function for a homogeneous layer (thickness = H) over a homogeneous half space with a water table at z = L (solution to Equation 1 with boundary conditions 3, 5, 6, and 7) is:

$$G(L>z>H,\omega) = \frac{\cosh[\alpha_2(L-z)]}{\cosh[\alpha_2(L-H)]\cosh(\alpha_1 H) + \kappa \sinh[\alpha_2(L-H)]\sinh(\alpha_1 H)} \qquad (12)$$

$$\text{where } \kappa = (k_2/k_1) \times \sqrt{C_1/C_2}$$

The Green's function can be used to determine the downhole pressure response of for any arbitrary surface pressure data set. In the frequency domain, this is simply a multiplication:

$$p_D(z,\omega) = G(z,\omega) \cdot p_S(0,\omega) \qquad (13)$$

In the time domain, this operation is represented by the convolution:

$$p_D(z,t) = \int_{-\infty}^{t} G(z,t-\tau)p_S(0,\tau)\partial\tau \qquad (14)$$

Note that in general, the subsurface pressure depends on the entire history of the surface pressure. For practical situations, we never have an infinitely long surface pressure record. It is sometimes assumed that the data lengths are long enough to approximate a stationary time series. In our interpretation technique, we also will assume that the data set is long enough to approximate a stationary time series.

Length of Impulse Response

The impulse response of the diffusive system can be very long. Figure 2 illustrates the impulse response for a homogeneous half space (k = 10 darcies, φ = 10%, C = $\approx$1600 m^2/hr) with a water table at 700 meters. Note that there is a significant contribution to the impulse response at depth out to times of about 300 hours (or 12 days). One of the effects of a long impulse response is that either the entire surface pressure history for time spans greater than this or the entire initial pressure distribution p(z,t=0) in the media must be known before gas transport predictions from transport models can be reliably made as the driving pressure for transport depends upon these initial pressure conditions. Figure 3 illustrates the decay of subsurface pressure with time for an initial subsurface pressure that is 0.1 psi greater than the surface pressure (surface pressure, p(0,t) = 0.0) in the homogeneous half space example of Figure 2.

Data Acquisition

Surface and downhole atmospheric pressures have been recorded from post-shot holes that were completed for gas sampling. The typical configuration is illustrated in Figure 4. The holes have been cemented around the tubing for a significant fraction of the total hole depth. The holes penetrate the cavity region and/or chimney region. The instrumentation consists of two high precision quartz pressure gauges. Both gauges are buried several feet under ground on the surface in order to reduce thermal effects upon the gauges. The subsurface pressure sensor is connected by hose to the interior of the post-shot hole tubing. The surface pressure sensor is connected to the atmosphere with a hose. A digital recorder (a modified Commodore SX-64 computer) samples the pressures every 10 seconds. The digital data stream is then desampled (with digital anti-alias filtering if desired) to a sample time interval of 30 minutes (2 samples/hour) and recorded on a floppy disk. A typical data set length is about 300 to 500 hours of data (12-21 days). This length was chosen by balancing the desire to instrument several different sites in a finite time period and the natural occurence rate for pressure fronts at NTS. The maximum length for continuous recording at 2 samples/hour is about 40 days; the size of the floppy disc on the computer determines this length.

Data Interpretation (Time Domain)

Several finite difference codes have been written to solve the diffusion equation with the boundary conditions for the geometry appropriate to post-shot completion (length of cement and total depth of hole) [7]. These codes can take a large amount of CPU time for complicated geometries. Therefore, to rapidly get an estimate of the bulk diffusivity of the chimney region, we initially interpret the data assuming a homogeneous medium. An iterative forward modelling scheme in the time domain is used to match the subsurface data using the surface data as input. The iterative calculation is terminated when the value of chi-square for the fit between the measured subsurface data and the predicted subsurface data does not change significantly. The data gathered to date are in Table 1.

The surface (or elevation of the ground surface in the models) was assumed to be the elevation of the post-shot hole. However, this is not always a good assumption. A large surface crater that is 25 meters deep means that the subsurface pressure sensor is 25 meters closer to the boundary where the surface pressure is applied than we assumed in the interpretation. For the Agrini site with its bottle-shaped crater 68.6 meters deep, we also interpretated the data with the surface sensor being 68.6 meters closer to the subsurface sensor and obtained 1374 m^2/hr (a reduction of about 50%). Assuming a porosity of 10%, the range of diffusivities calculated (132-31000 m^2/hr) correspond to a permeability range of about 1-200 darcies. For volcanic rocks, laboratory measured matrix permeabilities are typically in the millidarcy range. The large values for the Pahute Mesa sites (U19ac, U20am, U20ap) would indicate that a combined fracture-matrix bulk diffusivity is being estimated and not just a matrix diffusivity. It should be noted that calculating the permeability from our estimates of diffusivity requires that the value of connected porosity be known. In general, the porosity is not known very well. Estimates range from less than 1% for volcanics to 30% for alluvium at NTS.

Table 1

Estimates of Chimney Diffusivity from Independent Pressure Data Sets

Hole	Event	Independent Diffusivity (m^2/hr) Estimates			Depth of Cement (m)
U2et	Cheedam	312			194.5
U2ev	Agrini	2790	2288	1374 **	117.3
U2##		414	398	384	214.0
U2fd	Tarko	1335			242.9
U2ff	Laban	182	188		200.6
U4ar	Breton	132			333.5
U8c	Norbo	400			217.6
U19ac	Tierra	3599			387.0
U20ac	Colwick	7412			557.0
U20am	Kappeli	30000	31000		495.0
U20ap	Bodie	551	415		202.1

** using crater depth of 68.6 meters as the elevation of the surface sensor.
U2## is an unannounced event in alluvium.

Data Interpretation (Frequency Domain)

We have also developed a method to rapidly estimate the diffusivity using a frequency domain representation of the data. The method assumes that the data sets are long enough to approximate a stationary time series. This method is quite simple. First, we calculate in the frequency domain the complex transfer function between the surface and subsurface pressure data (The complex transfer function is the impulse response of the system or the Green's function for a delta function pressure input.). Second, from the amplitude of the complex transfer function, we calculate an apparent diffusivity by using the following transformation:

$$C_{apparent} = \frac{\omega z^2}{2 (\ln |\text{transfer function}|)^2} \qquad (15)$$

where $|\ |$ is the modulus of the complex transfer function.

This transformation is based upon the modulus of the Green's function for a homogeneous half

space without a water table (Eq. 9). The $C_{apparent}$ transformation has several advantages over the transfer function as a means of representing the data. First, the units are the same as the desired physical property. Second, for a nearly homogeneous earth without a water table, the $C_{apparent}$ curves will be constant and have the value of the diffusivity of the earth. Third, the $C_{apparent}$ curves are in general simpler than the transfer function, and changes in their curvature define frequency ranges where different zones in the earth are influencing the data. A similar transformation is routinely used to simplify the interpretation of electrical resistivity data.

Theoretical master curves were calculated for a measurement at a depth z in a homogeneous half space of diffusivity, C, with a water table (Eq. 10). Figures 5 and 6 plot the apparent diffusivity, $C_{apparent}/C$, and the phase as a function of $\omega z^2/C$ for different ratios of the water table depth, L, to measurement depth, z. To determine the diffusivity from a real data set, we obtain the complex transfer function by dividing the complex Fourier transform of the subsurface pressure data by the complex Fourier transform of the the surface pressure data. We transform the transfer function according to Equation 15 and then determine which theoretical curve best fits our data. For the phase data, we simply plot our data and then determine which theoretical curve best fits our data.

Let us illustrate this process with an real example. Atmospheric pressure data from U2## ($\approx$360 hours long) are shown in Figure 7. The "glitches" in the data correspond to data drop outs in the raw data stream. We have not removed these "glitches" in our interpretation of these data. These data had the mean and a linear trend removed and have been Fourier transformed into amplitude and phase spectra. Figure 8 gives the amplitude spectrum of the surface and subsurface data along with an estimate of a transfer function calculated by dividing these two spectra. Note that the U2## data have power in a frequency band from about 0.004 to 0.025 cycles/hour. Data at lower frequencies give a physically unreasonable transfer function value that is greater than 1.0; data at higher frequencies do not appear to have much power (this is particularly true in the subsurface pressure sensor data). The amplitudes are partially transformed in Figure 9 and the phase differences are displayed in Figure 10.

In order to obtain diffusivity using Figure 5 as an interpretation tool, we need to know the depth of the downhole pressure sensor. Hanson [7] has shown that it is a good approximation to use the midpoint between the bottom of the cement and bottom of the post-shot hole as the depth of the subsurface pressure sensor. Figure 9 gives a value of about 0.0055 for $C_{apparent}/Z^2$. With Z=267.3 m, the flat portion of the curve in Figure 9 ($C_{apparent}/C$ = 1.0) yields a value of 393 $\pm$ $\approx$50 m^2/hr (error based upon scatter in plot) for a homogeneous half space model. The value of 393 m^2/hr compares favorably with the average value of 397 m^2/hr calculated with the time domain finite difference technique for the same data set. The phase difference plot for a homogeneous half space model also gives diffusivity values in this range.

Limitations of the Frequency Domain Diffusivity Estimation Technique

The pressure data have a limited spectrum; our data have a frequency range (0.002-0.03 cycles/hr) for useful information. Above 0.03 cycles/hour (or periods shorter than about 33 hours), there are significant sources of "noise" from solid earth tides which do not obey Eq. 1 and thermal effects on the sensors. At frequencies lower than 0.002 cycles/hour (or periods longer than 500 hours), the data sets that we typically obtain are just not long

enough (most data sets are between 350-500 hours long). The driving factor in determining the length of data to record is the natural weather cycle at the NTS which produces the atmospheric pressure changes that we are interested in exploiting. Typically, an atmospheric pressure front (storm) typically occurs every 2-5 days at the NTS. This corresponds to pressure data in the frequency range of 0.008-0.02 cycles/hour. The data length that we can continuously record is limited by the size of the floppy disc to a maximum of about 40 days and by our "boredom factor" in wanting to acquire data in a finite time period. Fortunately, the natural weather cycle falls in between the time periods that we would get "bored" in gathering the data and the ones where the signal is contaminated.

These limits on frequency put real constraints upon our ability to resolve the diffusivity for a model and in our ability to distinguish between the simple models that we have proposed as interpretation aids. The plots of the theoretical Green's functions enable us to examine the uniqueness and resolution capabilities of the method. The conclusions that can be drawn from these plots would apply to the time domain results as well as any frequency domain results.

The frequency limitations mean that we can only put a lower bound on the depth of the water table and that we cannot use the data to determine the absolute depth of the water table. The locations of the bends in the curves in Figure 5 are the diagnostic tool for determining the depth of the water. For the U2## case, the data fell on the flat portion of the curves in Figure 5 (the ratio, $C_{apparent}/C = 1.0$). The smallest value of $\omega Z^2/C$ (for f = 0.004 cycles/hr) is about 4.5; thus the water table depth, L, must be greater than about 1.5 Z (or 400 m).

Two Layer Models

In the U2## example, we interpreted the data assuming a homogeneous half space. One can also ask: Do the data support a two-layer model interpretation? The interpretation process is somewhat more complex for the two layer model. First, master curves are constructed for the model under consideration. The parameters of the model are the diffusivities of the two layers, the permeabilities of the two layers, the thickness of the top layer, the depth to the water table, and the depth of the subsurface pressure sensor. One could construct master curves for apparent diffusivity as a function of these parameters; however, this would be a large number of plots. One possible way to proceed is to restrict the parameter space by using geologic knowledge of the problem under consideration. For example, the depth to the water table, the depth of the subsurface pressure sensor, and the thickness of the first layer could be constrained or even determined from geologic investigations. To illustrate the methodology, we have constructed a set of master curves for apparent diffusivity (Figure 11) and phase response (Figure 12) for the example in Table 2. We have constrained the ratio of permeabilities to be the same as the ratio of diffusivities (the connected porosity of both layers is the same). After calculating the apparent diffusivity from the measured pressure data, one does curve matching as was described in the previous section.

Examination of Figure 11 reveals some interesting features. Suppose that the apparent diffusivity data is basically constant (like the U2## example apparent diffusivity). Then the only diffusivity that we can really resolve is the diffusivity of the second layer, C_2. For example, suppose the apparent diffusivity is constant at 300 m^2/hr over the frequency band 0.004-0.02 cycles/hour. Then Figure 11 indicates the possibilities listed in Table 2.

Therefore, with apparent diffusivity data in the frequency band 0.004-0.02 cycles/hour, we would be unable to distinguish among any of the two layer cases listed in Table 2

that have a C_1/C_2 ratio greater than or equal to 1.0. The small ratios are excluded because their corner frequencies fall outside the frequency range from 0.004-0.02 cycles/hour. Even with this restriction, we cannot really resolve the top layer's diffusivity. The top layer's diffusivity ranges from 300-78947 m^2/hour while the bottom layer varies over a range from 300-79 m^2/hour. It should be noted that we used the "eyeball" technique to determine where the curves in Figure 11 become "flat". Closer inspection might change the corner frequencies some; however, the effect is still the same. The ability to resolve the diffusivity of the top layer of a two-layer system with the pressure sensor in the second layer is severely limited (when the top layer is more diffusive and the apparent diffusivity data is band limited to a frequency range that corrsponds roughly to the atmospheric weather patterns). We are only really able to determine the smaller of the two layers' diffusivities.

Table 2

C_1/C_2	$C_{apparent}/C_1$	C_1	C_2	Corner Frequency (cycles/hour)
1000.0	0.0038	78947	79	0.003
100.0	0.033	9091	91	0.003
10.0	0.23	1304	130	0.003
1.0	1.0	300	300	0.003
0.1	2.2	136	1360	0.13
0.01	3.1	96	9677	1.9

$C_{apparent}$ = 300 m^2/hr

All diffusivities in m^2/hr

Depth of sensor = 400 m

Thickness of first layer = 200 m

Depth of water table = 600 m

Ratio of layer permeabilities is equal to the ratio of layer diffusivities.

Corner frequency is the frequency above which the apparent diffusivity data are flat for that particular C_1/C_2 ratio.

Figure 13 is an expanded version of Figure 11 for low ratios of C_1/C_2. Here the curves are not quite flat. However, the ability to distinguish between the master curves beyond a ratio of 0.01 is almost impossible. This means that when the top layer is more than 100 times less diffusive than the second layer for the parameters of the two layer model of Table 2, it would also be impossible to resolve the diffusivity of the bottom layer.

Effect of the Water Table

The water table takes up volume that would otherwise be a sink or source of air. The

effect of the water table is readily seen in Figures 14, 15, 16, and 17. At high and very low values of $\omega Z^2/C$, the ratio of the Green's functions with and without a water table is unity as would be expected. At high frequencies, the pressure pulse never "sees" the water table as the water table is many diffusive "skin depths" deep. At very low frequencies, the pressure in the medium has time to equilibrate throughout the medium. In the intermediate frequency range, there is some enhancement of the amplitude of the pressure response at depth at most frequencies and very surprisingly also some frequencies at which the response is less. This part of the result is not well understood; however, we speculate that there is some type of resonant condition (like standing waves) that reduces the response at these particular frequencies. The enhancement was expected as the pressure waves "see" the water table and cannot propagate beyond it. For an impulse at the surface, the pressure response at depth would tend to build up more rapidly than if the volume below the water table had been available for storage of air.

Summary

Analytical expressions for the Green's functions of several simple models were calculated to aid in the interpretation of atmospheric pressure data for diffusivity structure.

The length of the impulse response for a typical NTS geologic setting can be quite long (>300 hr). The surface pressure history for time spans greater than 300 hr or the entire initial pressure distribution in the medium must be known before gas transport predictions can be reliably made from transport models, as the driving pressures for transport depend upon these initial conditions.

The range of diffusivities of chimneys measured to date is 132-31000 m^2/hr. These were calculated using a time domain finite difference technique. The bulk diffusivities calculated with the atmospheric pressure technique are a measurement on a large volume of material. The measurement includes the effect of the matrix and any fractures that might be present. The range of values for and the ability to resolve bulk diffusivity are important because bulk diffusivity is a key parameter in gas transport prediction models.

A frequency domain technique for estimating diffusivity has been developed. Examination of the master curves from this technique enable bounds to be established for our ability to estimate diffusivity. In two layer models, we can only resolve the smaller of the two layers' diffusivities.

The effect of the water table upon our data has been studied. In the intermediate frequency range, the presense of a water table near the downhole sensor enhances the pressure response.

Acknowledgements

This work was supported by the Nuclear Test Containment Program at Lawrence Livermore National Laboratory. It was performed under the auspices of the U. S. Department of Energy under Contract Number W-7405-ENG-48. Norman Burhard would like to acknowledge the very useful discussions with and stimulation provided by Paul Kasameyer on the interpretation methodology presented.

References

1. Nilson, R. H. and Lie, K. H., Numerical analysis of oscillatory gas motion and contaminant transport in a fractured porous medium, presented at the 4th Containment Symposium, this volume, 1987.
2. Nilson, R. H., Lie, K. H., and Peterson, E. W., Fickian filtering of cavity gases rising through a fractured permeable overburden, presented at the 4th Containment Symposium, this volume, 1987.
3. Hanson, J. M. and Hearst, J. R, Evaluation of permeability in the unsaturated zone at the Nevada Test Site using barometric pressure modeling, Proceeding of the Third Symposium on Containment of Underground Nuclear Explosions, Volume 1, LLNL CONF-850953, p. 392.
4. Rozsa, R. B., Snoeberger, D. F., and Baker, J., Chimney permeability data analysis, LLNL Report UCID-16440, January 30, 1974.
5. Snoeberger, D. F., Baker, J., Morris, C. J., and Rozsa, R. B., Permeability of a nuclear chimney and surface alluvium at the AEC Nevada Test Site, LLNL Report UCID-16479, April 17, 1974.
6. Snoeberger, D. F., Baker, J., Morris, C. J., Measurements and correlation analysis for nuclear chimney permeability, LLNL Report UCID-16302, July 10, 1973.
7. Hanson, J. M., Barometric pressure transient testing applications at the Nevada Test Site: Formation permeability analysis, TerraTek Report to LLNL, December, 1984, UCRL-15699.

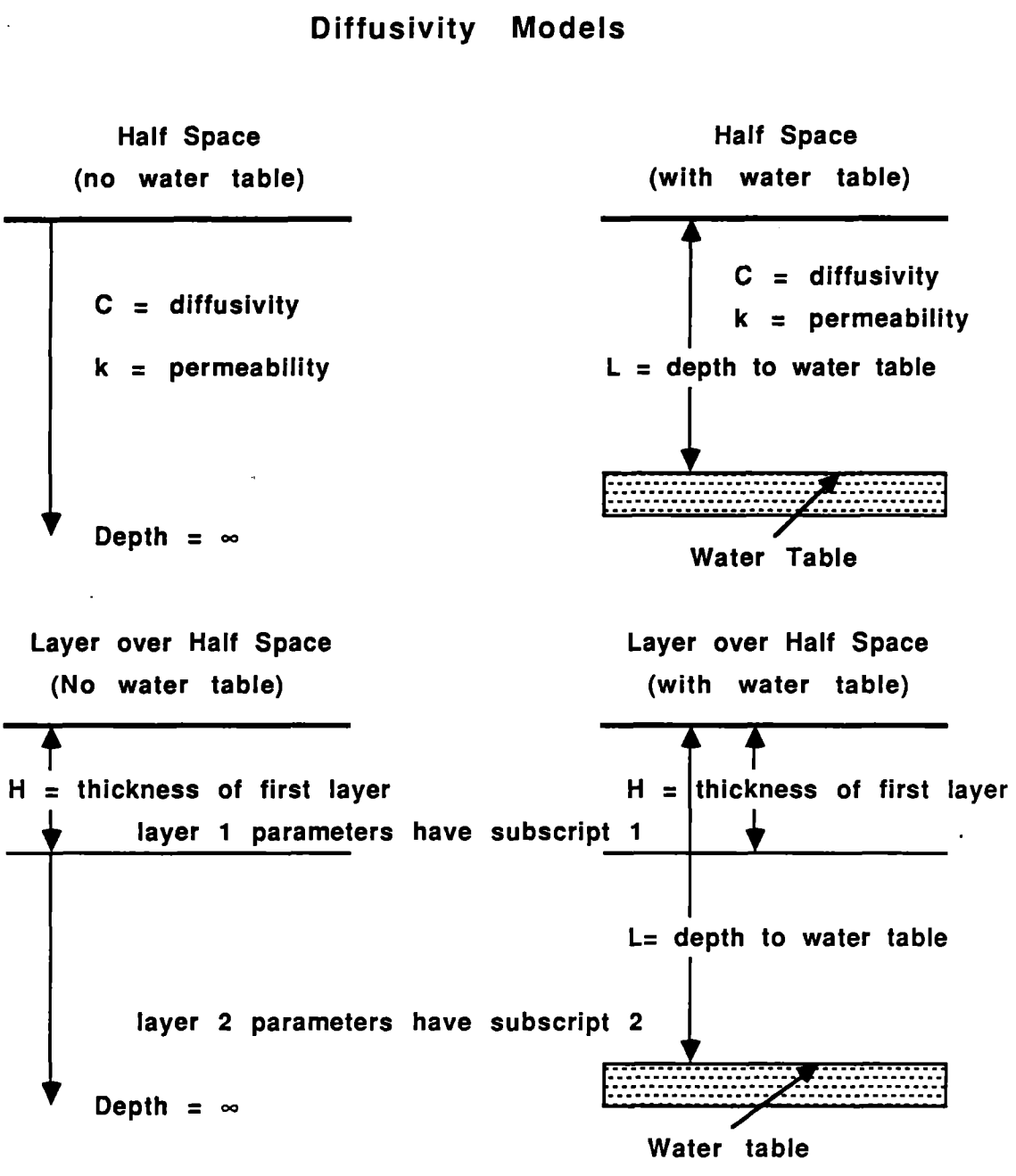

Figure 1. Models used in Green's function calculations

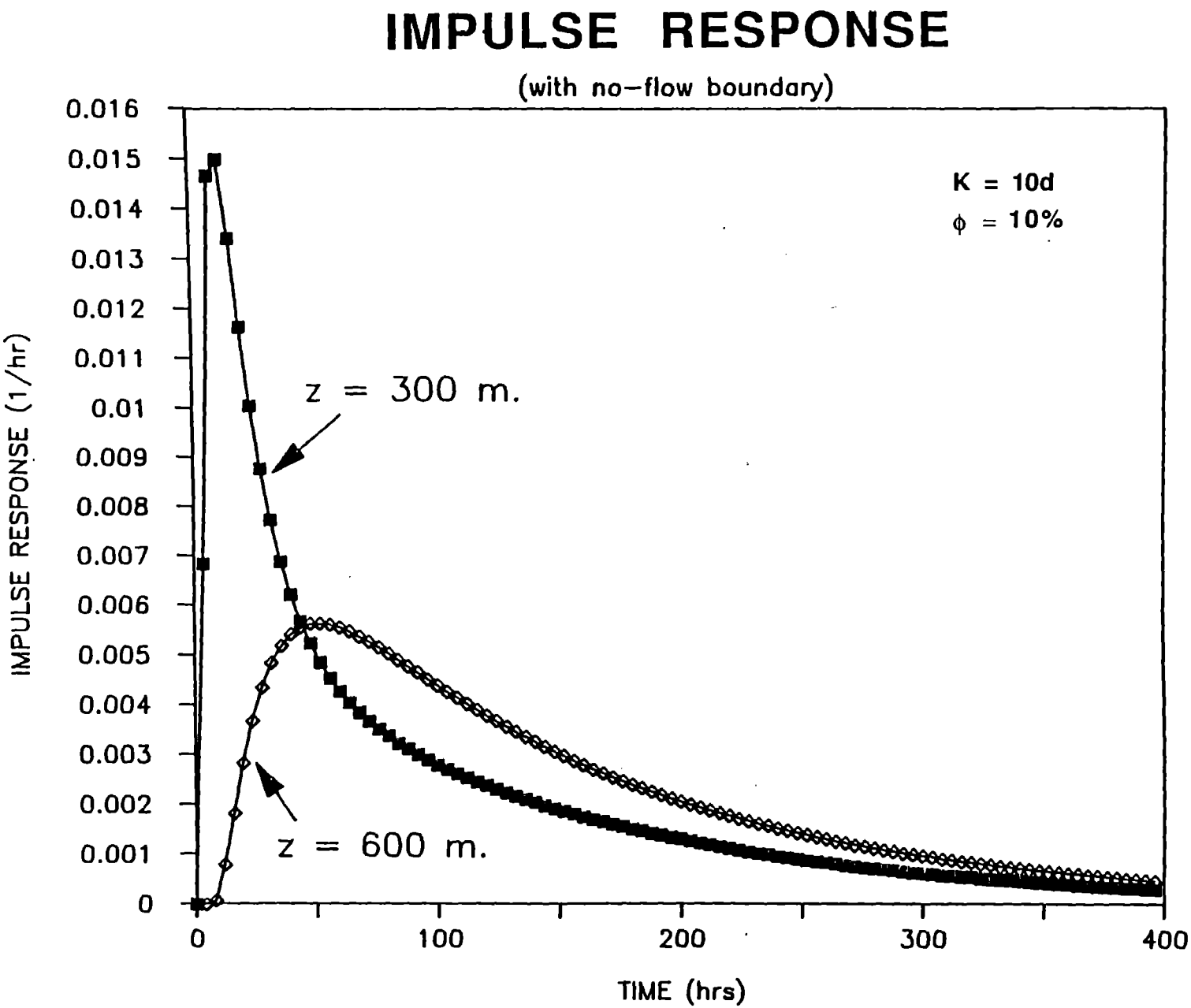

Figure 2. Impulse response (Green's function) of half space with a water table at 700 m. Subsurface sensors are located at 300 and 600 m.

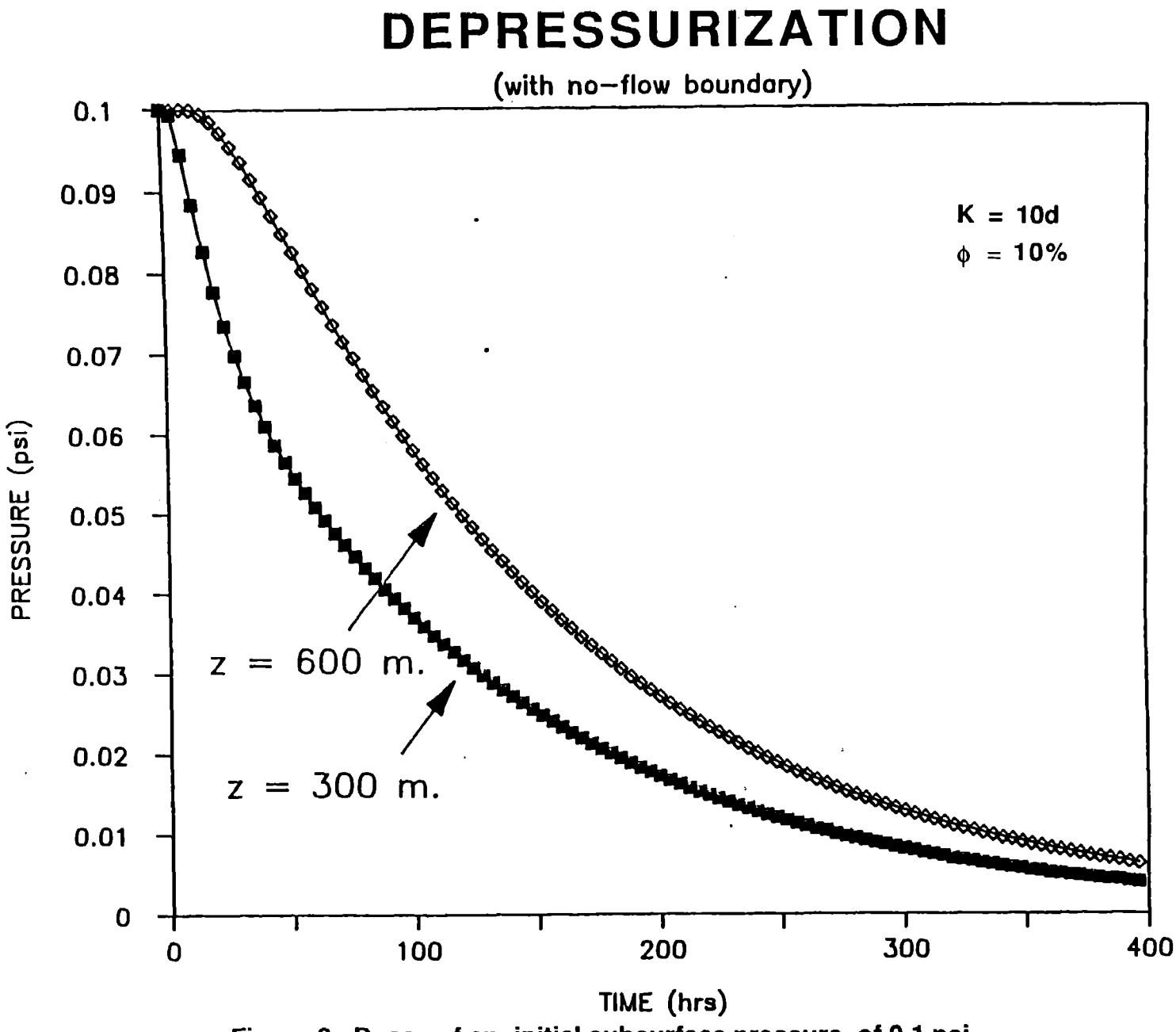

Figure 3. Decay of an initial subsurface pressure of 0.1 psi for a half space with a water table at 700 m with surface pressure held at 0.0 psi. Subsurface sensors are located at 300 and 600 m.

Figure 4. Schematic of gas sampling post shot hole used for atmospheric pressure measurements.

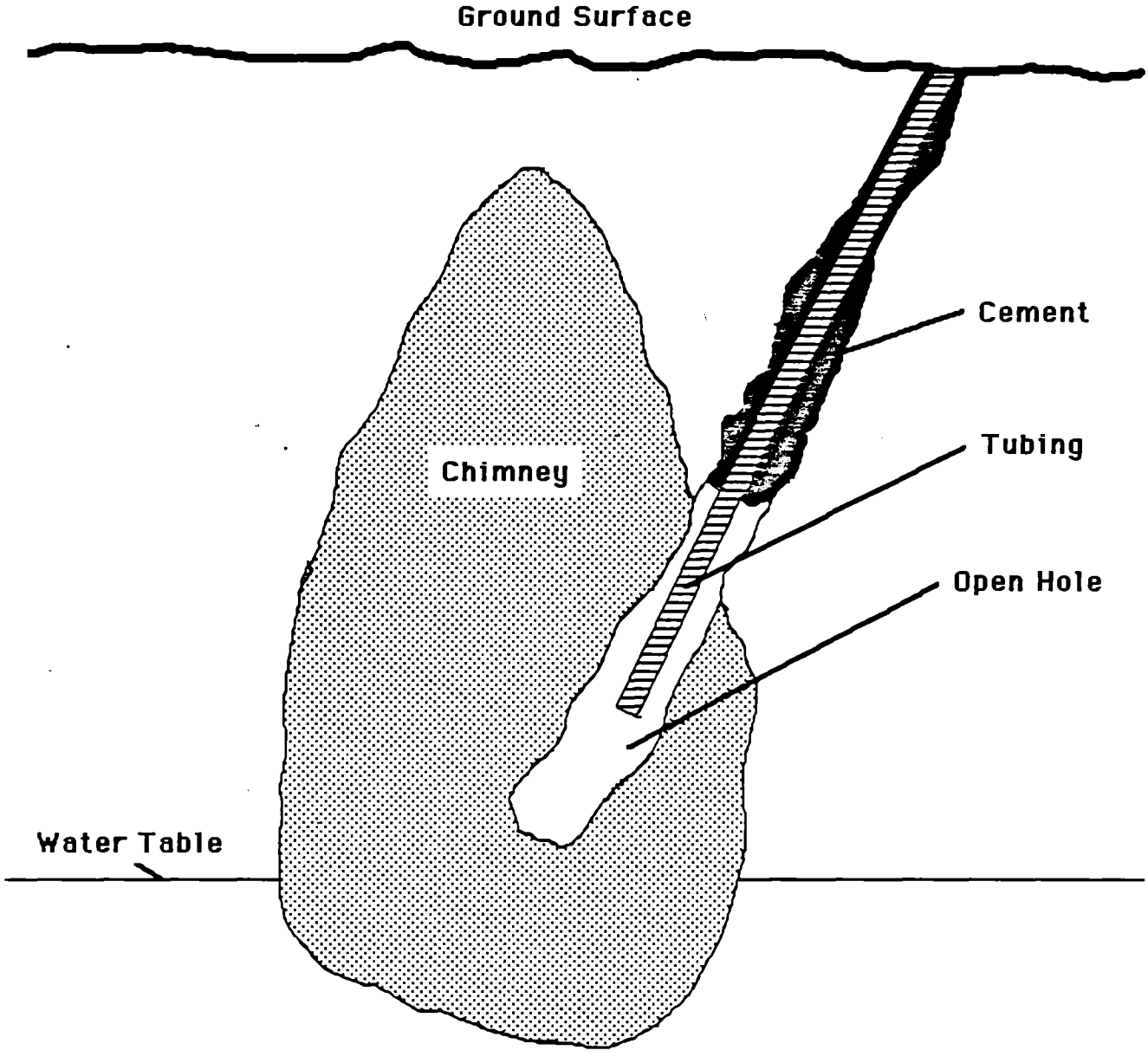

Figure 5. Theoretical master curve for apparent diffusivity in a half space of diffusivity, C, for a measurement at depth, z, with a water table at depth, L.

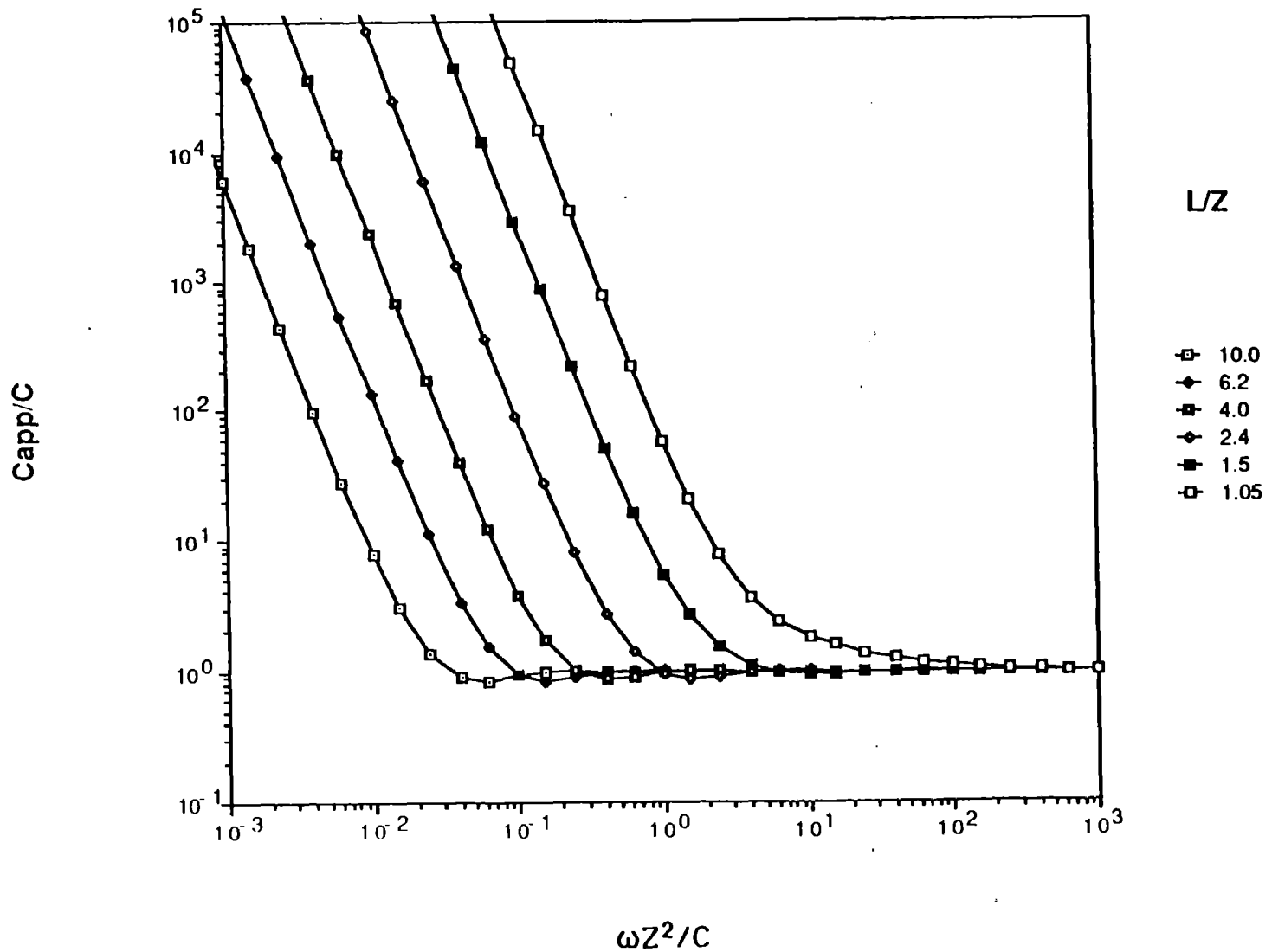

Figure 6. Theoretical master curve for the phase response in a half space of diffusivity, C, for a measurement at depth, z, with a water table at depth, L.

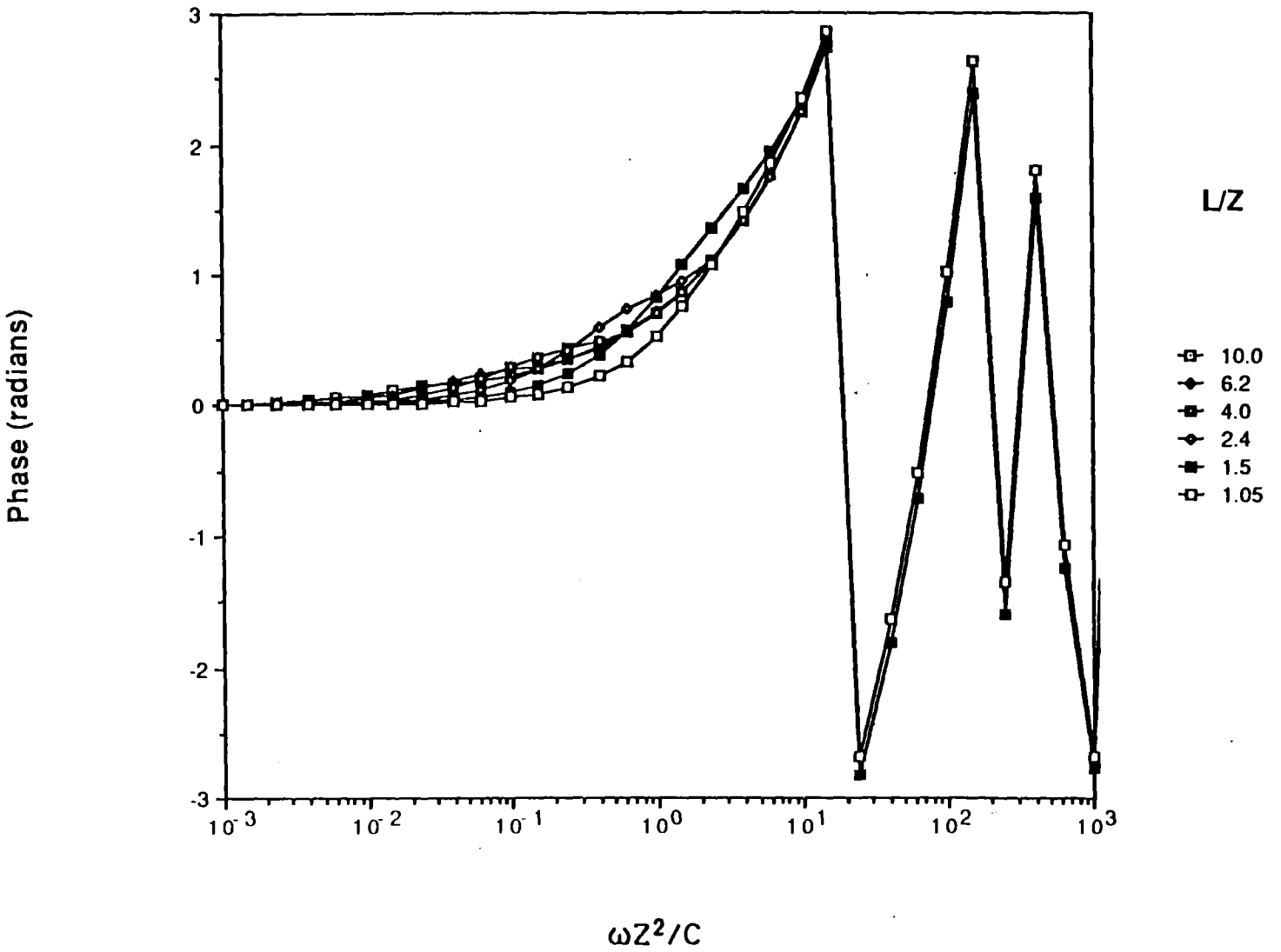

Figure 7. U2## atmospheric pressure variations

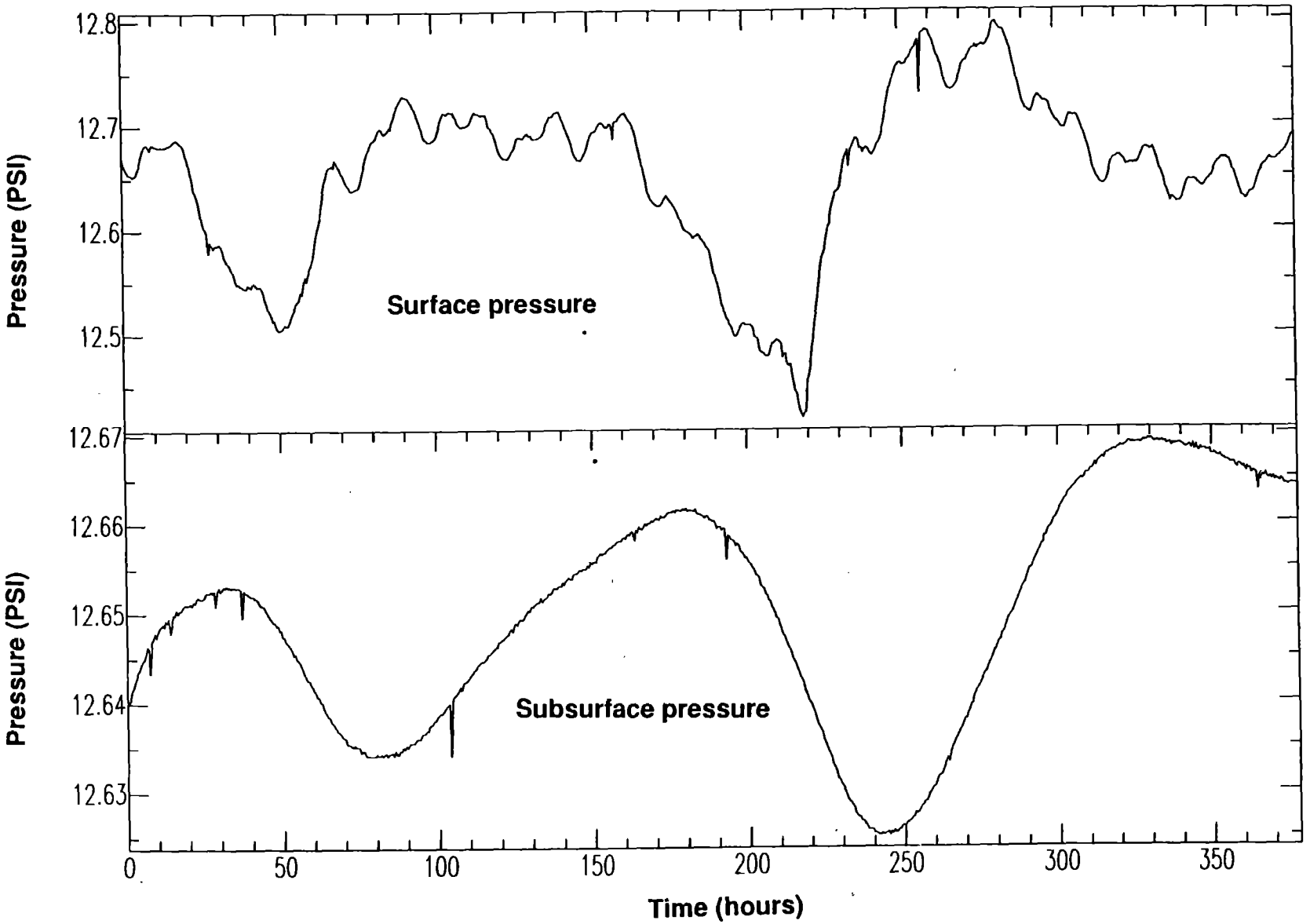

Figure 8. U2## transfer function and amplitude spectra

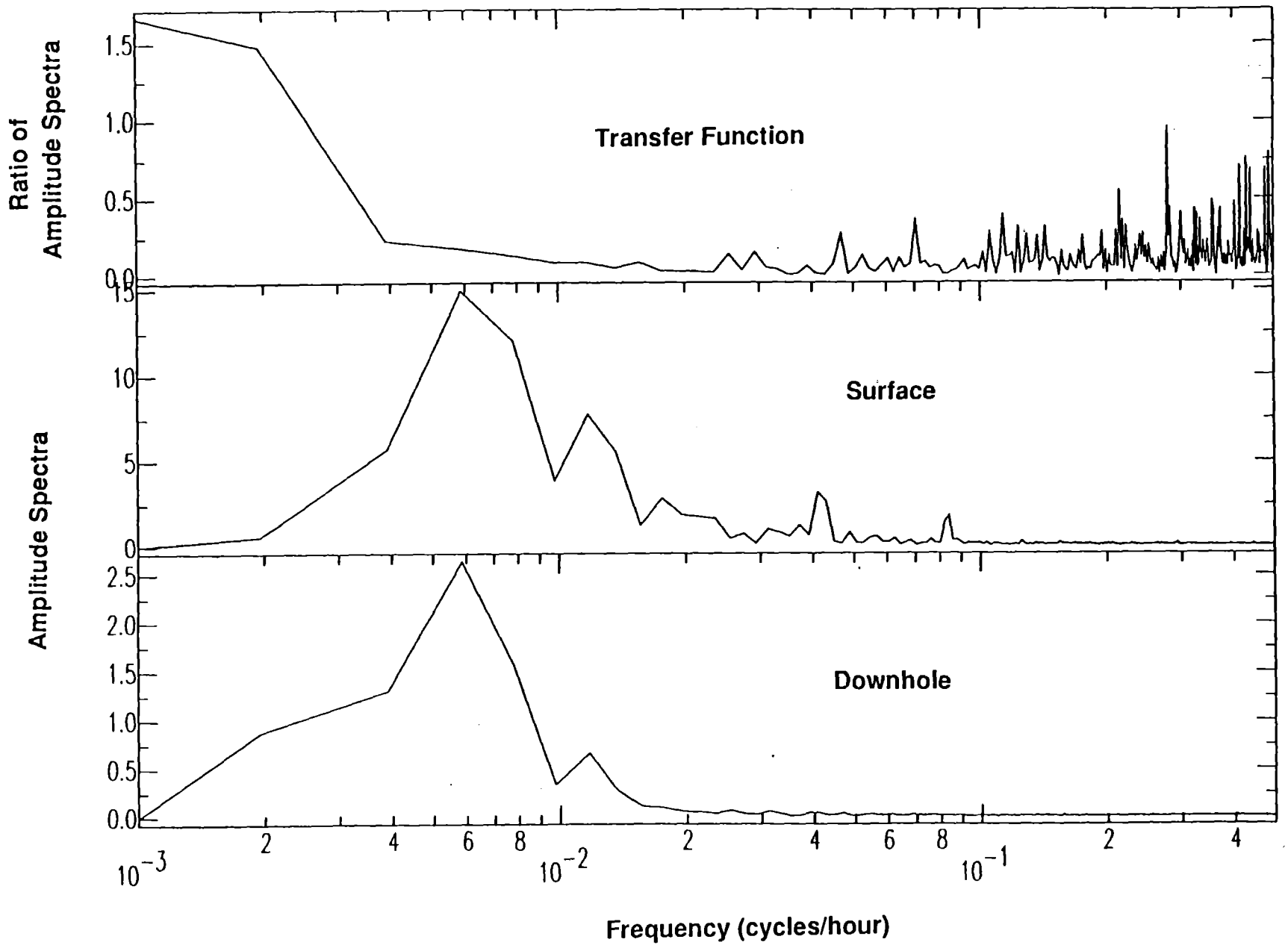

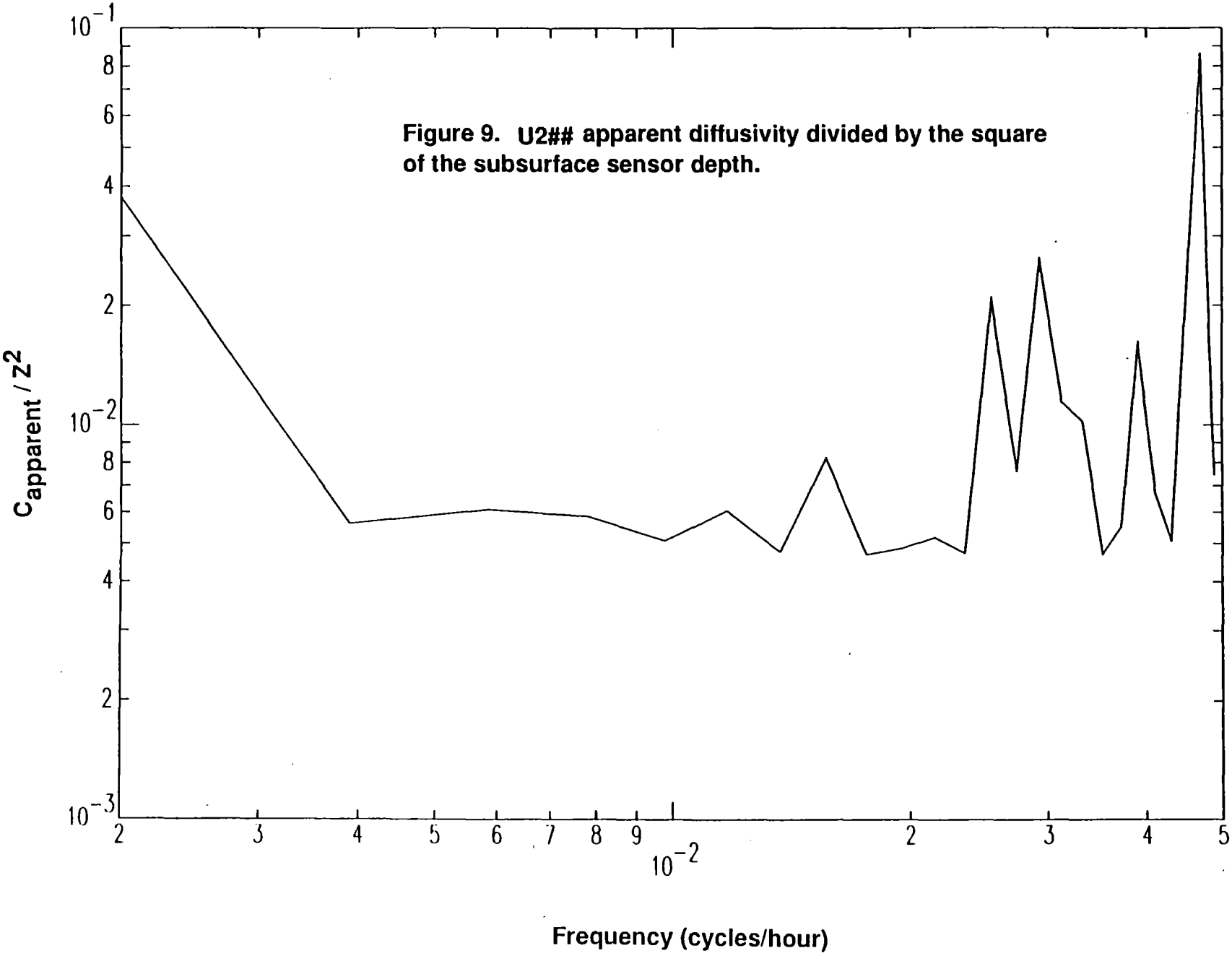

Figure 9. U2## apparent diffusivity divided by the square of the subsurface sensor depth.

Figure 10. U2## phase differences between the surface and subsurface sensor.

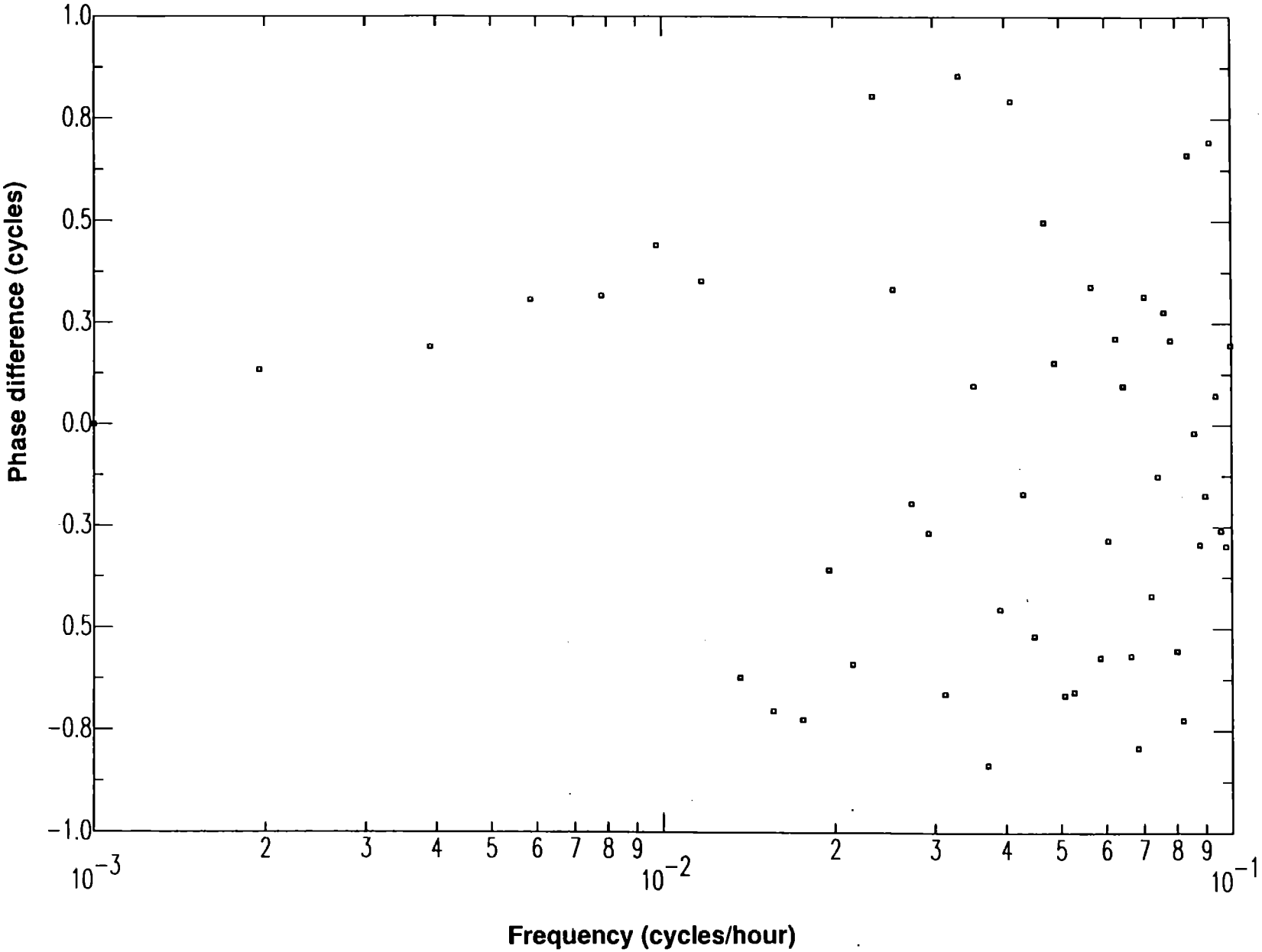

Figure 11. Theoretical master curve for the apparent diffusivity, C, for a two layer model with a water table. The model used to construct these curves is listed in Table 2.

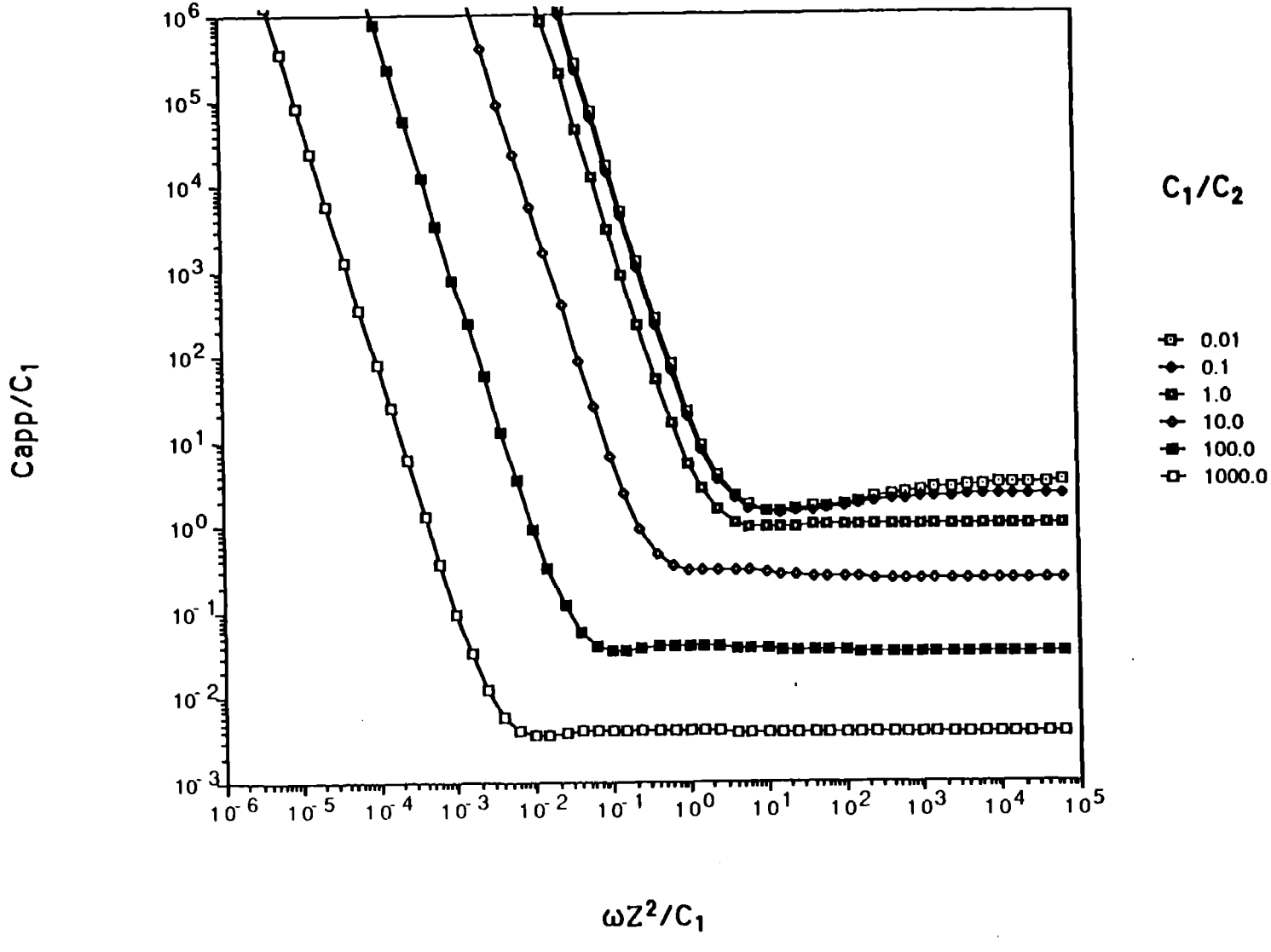

Figure 12. Theoretical master curve for the phase response for a two layer model with a water table. The model used to construct these curves is listed in Table 2.

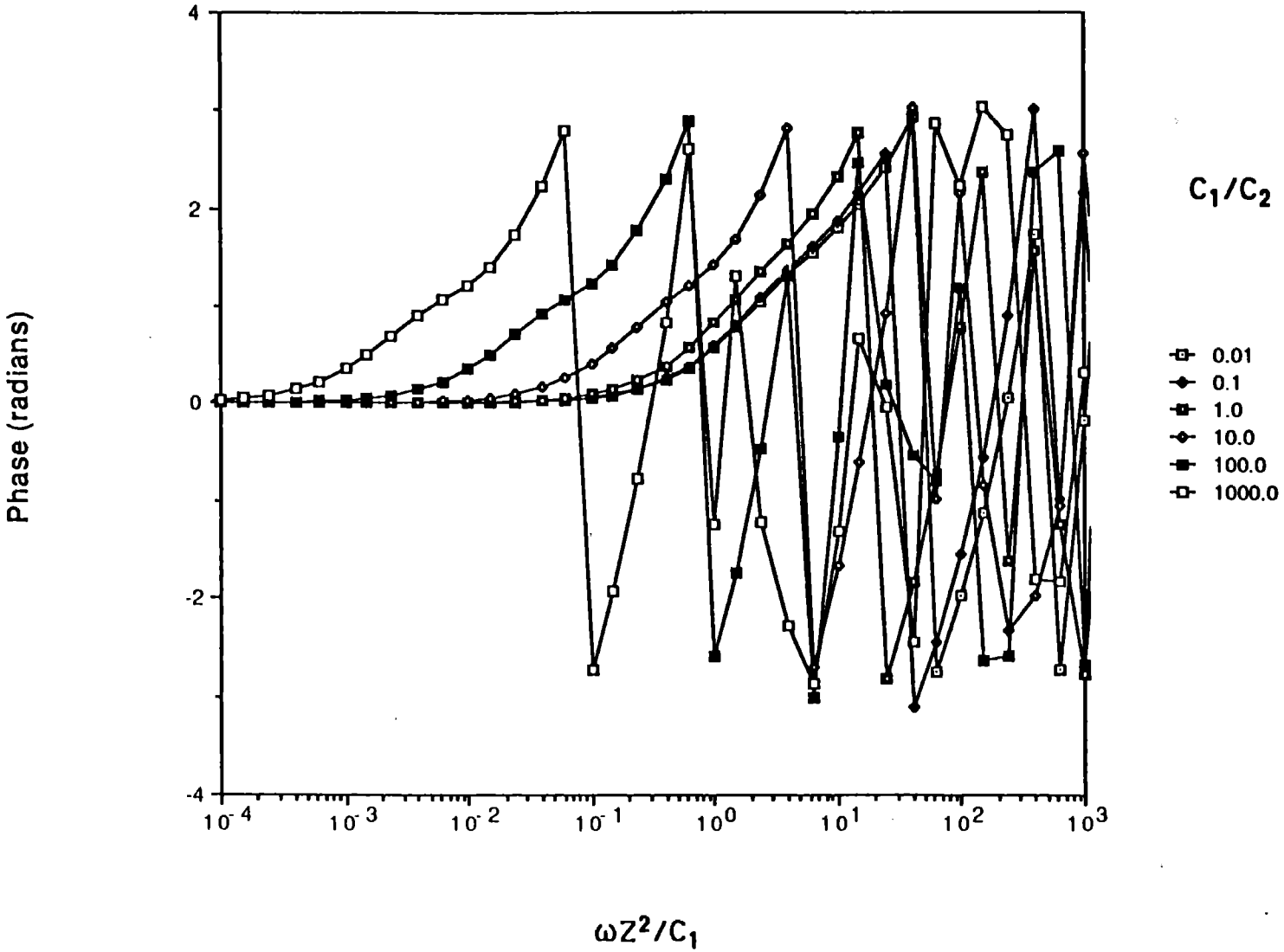

Figure 13. Theoretical master curve for the apparent diffusivity, C, expanded for small ratios of C_1/C_2 for a two layer model with a water table. The model used to construct these curves is listed in Table 2.

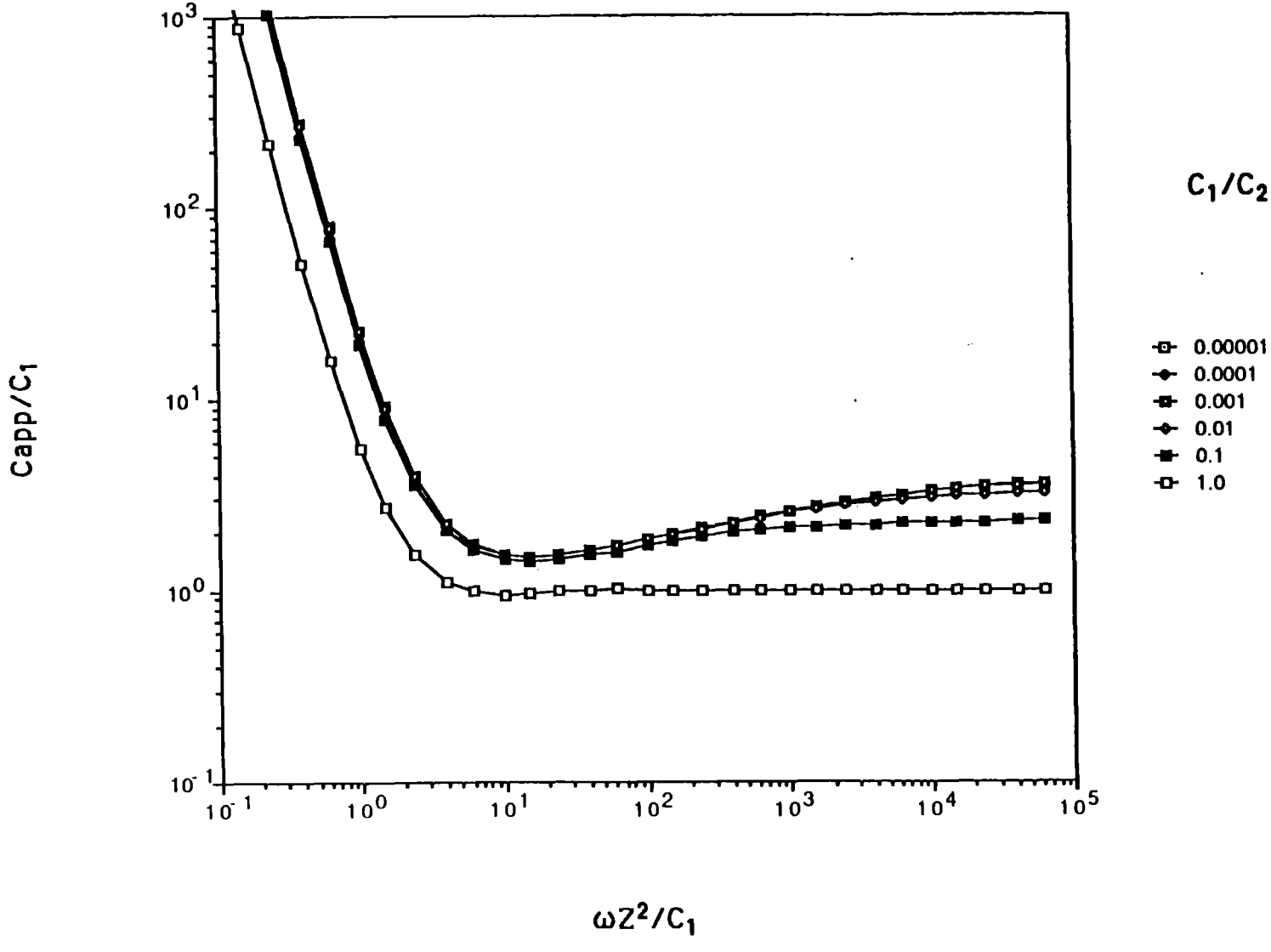

Figure 14. Amplitude ratio of Green's functions for homogeneous half space models with and without a water table.

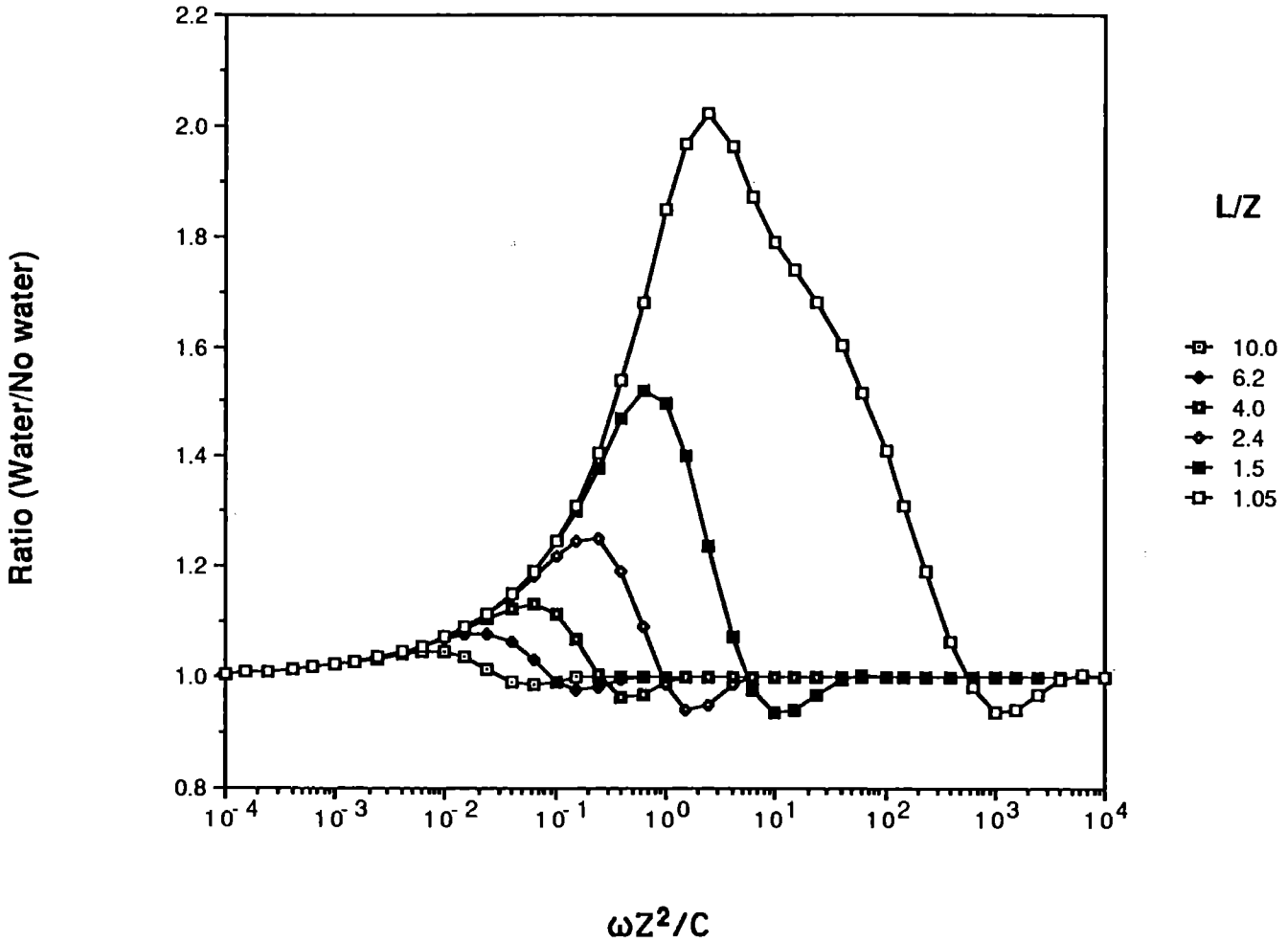

Figure 15. Phase difference of Green's functions for homogeneous half space models with and without a water table

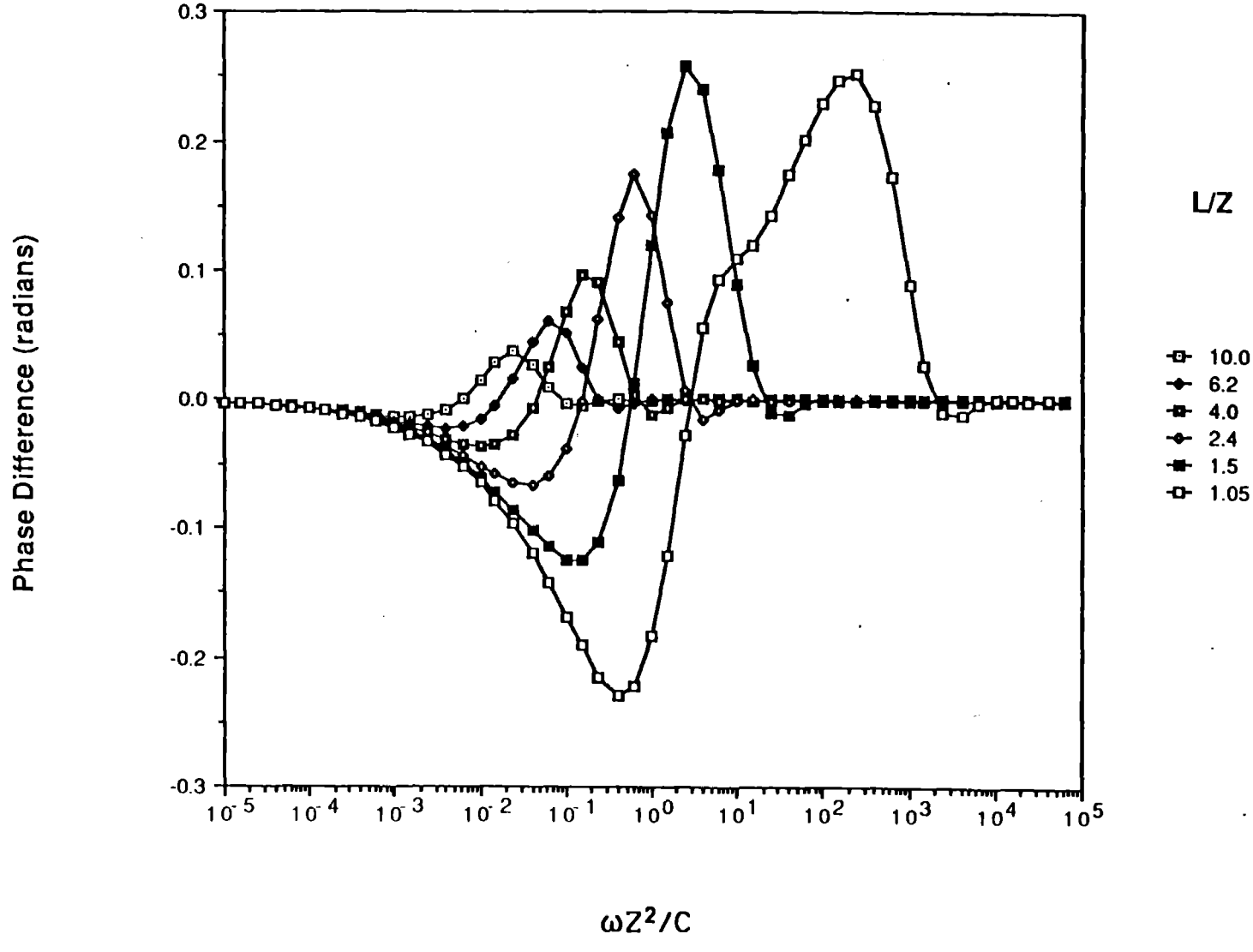

Figure 16. Amplitude ratio of Green's functions for two layer models with and without a water table. The model parameters are listed in Table 2.

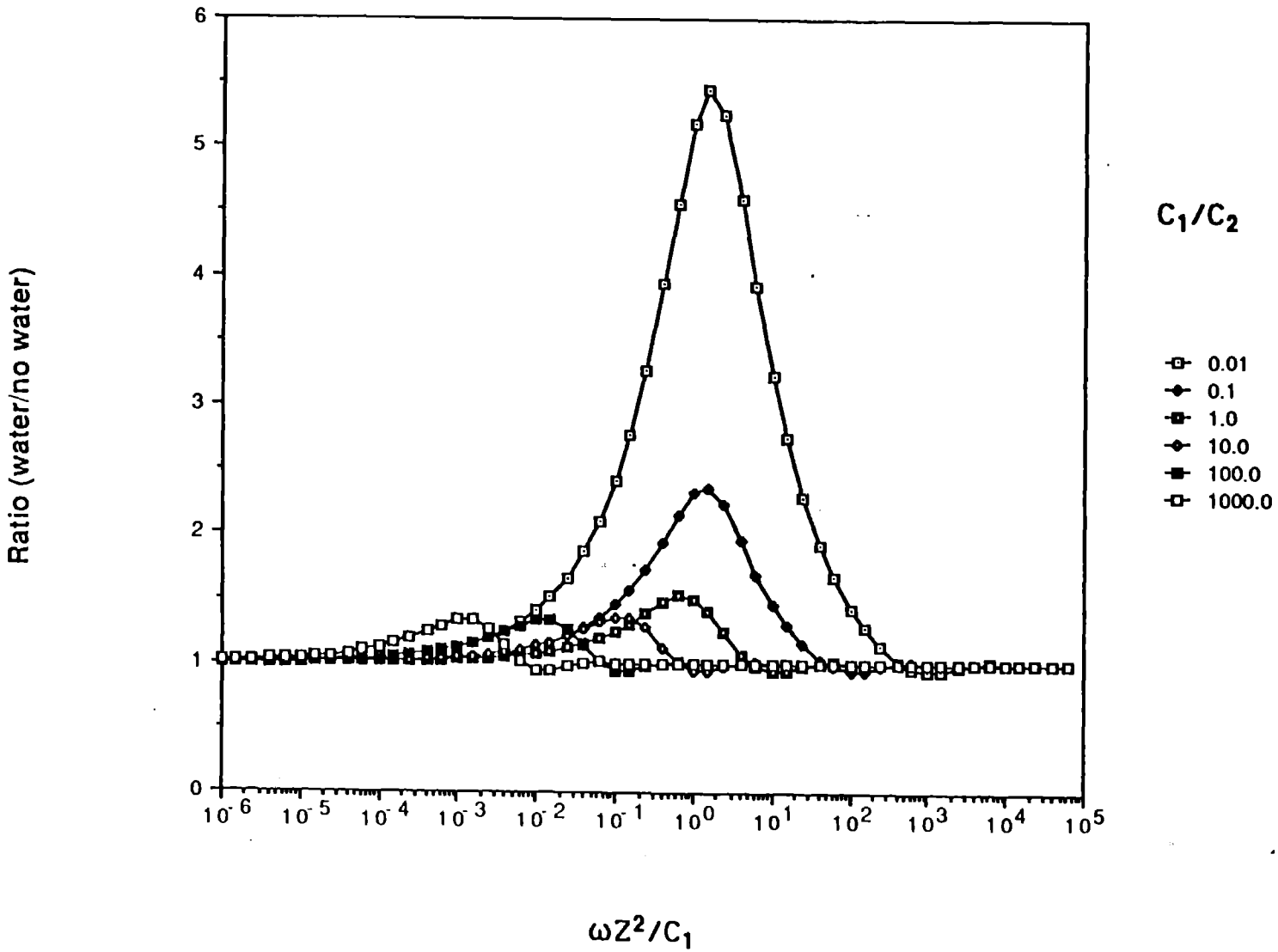

Figure 17. Phase difference of Green's functions for two layer models with and without a water table. The model parameters are listed in Table 2.